International Journal of Power and Energy Systems, Vol. 46, No. 10, 2026
An Open Access Paper

ENERGY STORAGE CONTROL OF NEW ENERGY DC MICROGRID BASED ON IMPROVED LION SWARM ALGORITHM AND VARIATIONAL MODE DECOMPOSITION ALGORITHM

Fanhua Meng,* Likui Yi,* Rui Feng,* Dongge Liu*

Abstract

The new energy photovoltaic Direct Current (DC) microgrid system is highly susceptible to environmental factors, leading to substantial nonlinearity and fluctuations in its output power. This situation severely constrains its stable operation and energy utilization efficiency in complex application scenarios. Consequently, this study initially enhances the traditional lion swarm algorithm by employing Tent mapping and dynamic probability factors to efficiently track the maximum power point of new energy DC microgrids. Subsequently, by integrating the Grey Wolf Optimizer algorithm with variational mode decomposition, frequency domain decomposition of the output power of new energy photovoltaics is conducted, ultimately attaining precise energy-storage control and dynamic compensation for high- and low-frequency power. The results indicate that under standard lighting, local occlusion, and dynamic change conditions, the research algorithm can achieve maximum power point tracking within 0.04 s, 0.064 s, and 0.35 s, respectively, reaching power peaks of 859.2 W, 581.6 W, and 614.9 W. The tracking accuracy is improved to 99.91%, 99.91%, and 99.89%. Compared with other algorithms, the research algorithm exhibits significant advantages in response speed, dynamic stability, and oscillation control. Moreover, after implementing the research method, the number of charge-discharge switching times of the battery pack is notably reduced to only 22 times. In conclusion, the research method not only shows superiority in maximum power point tracking performance but also realizes efficient integration and allocation of multi-source fluctuating power in energy management, presenting favorable practical prospects for promotion.

* School of Electric Engineering, Shenyang Institute of Engineering, Shenyang, 110136, China; e-mail: 13082203730@163.com, yi.likui@outlook.com, 15062152504@163.com, 18639583356@163.com
Corresponding author: Likui Yi
Recommended by: Amirthagunaraj Yogarathnam
(DOI: 10.2316/J.2026.203-0635)

Key Words

Lion swarm algorithm; Variational mode decomposition; Photovoltaic power generation; DC microgrid; Energy storage control

1. Introduction

With the large-scale integration of renewable energy, including wind and solar power, Direct Current (DC) microgrids have been widely used in industrial parks, military power sources, data centers, and smart building scenarios due to their advantages of simple structure, flexible power flow control, and high energy conversion efficiency [1], [2]. Nevertheless, DC microgrids still encounter numerous challenges during actual operation. These primarily encompass the volatility and intermittency of new energy power output, the high level of uncertainty in load-side demand, and the multiple constraints imposed on Energy Storage Devices (ESD) during the Charging and Discharging (C&D) processes [3]-[6]. To enhance the global optimization capability and dynamic response performance of new energy photovoltaic systems in complex environments, various intelligent optimization algorithms have gradually been introduced into Energy Storage Control (ESC) strategies. The Lion Swarm Optimization (LSO) algorithm has gradually become one of the research hotspots in power system optimization scheduling, parameter identification, and control strategy design due to its excellent global search ability, good adaptability, and fast convergence speed [7], [8].

For example, to achieve fast, energy-efficient, and reliable data transmission in DC microgrids, Silambarasan et al. proposed a multi-path fast routing scheme based on a hybrid simulated annealing and LSO algorithm. This algorithm effectively improved network throughput, prolonged the lifespan of the power system, and significantly reduced latency and Energy Consumption (EC) by selecting the optimal forwarding node that satisfied EC and delay con-

straints [9]. In terms of energy security and network optimization in DC microgrids, Dinesh et al. introduced the Grey Wolf Optimizer (GWO) algorithm for efficient node clustering. At the same time, it combined the LSO algorithm to achieve route optimization and ensured security by supporting conditional privacy of the uncertified set signature scheme and the elliptic curve encryption method. Compared with other existing protocols, the protocol reduced average EC by 12% and increased packet transmission rate by 8% [10].

Due to the strong nonlinear and non-stationary characteristics of new energy Photovoltaic Power (PVP) generation, there are complex fluctuations and frequency drift phenomena in signals such as voltage, current, and power in DC microgrids. Therefore, traditional signal processing methods are difficult to effectively decompose and extract features. Variational Mode Decomposition (VMD), as an emerging adaptive signal processing method, decomposes the original signal into several Intrinsic Mode Functions (IMFs) with finite bandwidth through a variational framework, enabling efficient and stable time-frequency analysis [11]. Li et al. proposed a signal processing method that integrated multi-delay embedding transformation, Tucker decomposition, and VMD to address issues such as short frequency sampling period and scarce measurement data in PVP plants. This method constructed a high-dimensional phase space feature matrix of the signal through multi-delay embedding. It used Tucker decomposition to achieve dimension compression and data enhancement, thereby effectively improving frequency resolution before frequency partitioning and providing more accurate feature support for subsequent VMD decomposition. Compared with traditional filtering algorithms, this method had significant advantages in frequency resolution accuracy and computational efficiency [12]. To address the impact of Wind Power Fluctuations (WPL) on power system stability, Zhang Y et al. proposed a VMD comprehensive control method that combines adaptive noise and a sliding window strategy. This method could timely smooth WPL and decompose Energy Storage Power (ESP) [13]. In islanded microgrids based on constant voltage and frequency control, nonlinear loads could easily lead to voltage harmonics, thereby reducing the islanded microgrids' power quality. To this end, Li et al. proposed an internal voltage robust control method for battery ESDs that suppressed broadband harmonics using VMD. This method could achieve voltage stability control of islanded microgrids under load disturbances [14].

In summary, traditional Low-Pass Filtering (LPF) or signal decomposition methods have limited accuracy in the power distribution process, with a fixed frequency cut-off, and are unable to effectively compensate for high-frequency fluctuations. Currently, various optimization and signal processing technologies have been introduced into the DC microgrid ESC. However, there are still problems, such as a lack of deep integration of optimization strategies and feature extraction mechanisms, and insensitivity to nonlinear dynamic characteristics, making it difficult to fully respond to the nonlinear dynamic characteristics of photovoltaic systems. Moreover, some methods still have limitations in terms of global search ability, convergence speed, and system robustness. In response to the above issues, the study has made innovative designs in the technical path: Firstly, it introduces Tent Chaotic Mapping (TCM) and a dynamic probability mechanism to improve the traditional LSO algorithm, and proposes an ESC strategy based on the improved LSO algorithm. Secondly, the GWO algorithm is adopted to improve VMD, and a hybrid ESP allocation strategy based on VMD-GWO is proposed. This strategy achieves fine power distribution and dynamic compensation by decomposing the mixed power signal into high-frequency and low-frequency components suitable for different energy storage components. Finally, by integrating the above two improvement methods, the collaborative optimization of photovoltaic MPPT and hybrid ESP distribution is achieved. Through this novel method, the study aims to provide a composite control scheme with high reliability, strong robustness, and high adaptability for the energy storage dispatching of new energy DC microgrids.

2. Methods and Materials

2.1 ESC Strategy for New Energy DC Microgrid Based on Improved LSO

This study is based on an independent PVP generation system and explores ESC strategies for new energy DC microgrids. Its topological structure is shown in Fig.1.

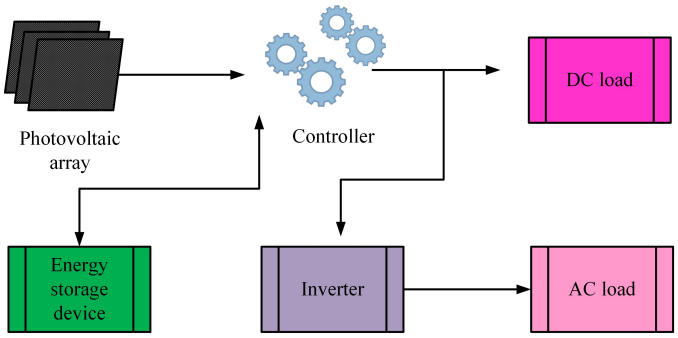

Figure 1. LSO Algorithm Process

In Fig.1, the system includes Photovoltaic Arrays (PVA), controllers, ESD, inverters, DC loads, and Alternating Current (AC) loads [15]. PVAs, as the main energy source in DC microgrids, are responsible for converting solar energy into DC electrical energy. The controller adjusts the output power of the PVA in real time to distribute energy, ensuring that the system operates close to the Maximum Power Point (MaxPP) under various operating conditions. Meanwhile, according to the specific electricity demand of the load, DC electricity is stored in ESDs or directly output to DC loads. After completing DC/AC conversion through inverters, it is supplied to AC loads for efficient power supply to different types of loads. Due to the susceptibility of PVP generation to external factors,

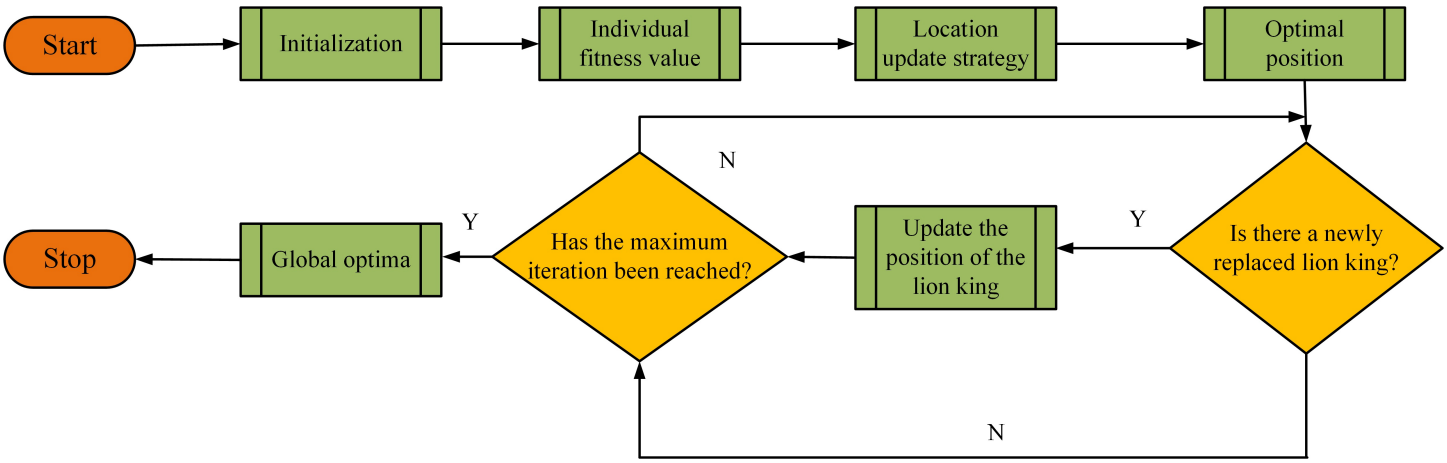

Figure 2. LSO Algorithm Process

including light and temperature, the Output Power Curve (OPC) of PVAs usually exhibits multi-peak characteristics, with only one globally optimal MaxPP [16] [17]. At present, the commonly used Maximum Power Point Tracking (MPPT) algorithms for PVAs mainly include Particle Swarm Optimization (PSO), the incremental conductance method, and the LSO algorithm [18]. Among them, the LSO algorithm can use the location information of individual optimal solutions to accelerate the search for global optimal solutions when facing multi-modal problems, thereby significantly improving the optimization efficiency [19] [20]. The LSO algorithm process is shown in Fig.2.

In Fig.2, LSO divides the population into three parts based on their fitness: lion king, lioness, and young lion. The individual with the highest fitness in the population is the lion king, who occupies the optimal position in the population. Individuals with moderate fitness are lionesses, who will randomly select another lioness for cooperative hunting. The individual with the worst fitness is the young lion, which randomly moves within the population, either approaching the lion king, following the mother lion, or being driven out of the lion pack. Firstly, the population size, individual dimensions, maximum iteration times, and the ratio of lion kings, lionesses, and cubs in the lion pack are initialized, and initial positions and velocities are assigned to each individual. Subsequently, through the fitness function, the fitness values of each individual are calculated, and roles are divided according to their strengths and weaknesses. To lift the global search capacity and convergence stability, the movement factor is dynamically adjusted during the iteration process, and the search step size is gradually controlled to shrink, so that the search center of gravity approaches the optimal solution region. The lion king, lioness, and cubs adjust their positions based on their respective update strategies, taking into account their current location and historical best position. During the process of evolution, the historical optimal solution of each individual is continuously recorded. After the update, individual fitness is re-evaluated. If a better individual is found, the current lion king will be replaced to maintain the global optimality of the population search direction. Finally, when the maximum iterations are reached, the optimal output position is the MaxPP in the current environment. The update formula for the dynamic movement factor α is given by Eq. (1).

$$\alpha = \alpha_{\max} - \frac{\alpha_{\max} - \alpha_{\max}}{T_{\max}} - t \tag{1}$$

In Eq. (1), α_{max} and α_{min} are the initial value and minimum of the movement factor. t is the current iteration count. T_{max} is the maximum iteration. The individual position update is given by Eq. (2).

$$X_i(t+1) = X_i(t) + \alpha \cdot \gamma \cdot (X_{best} - X_i(t)) \tag{2}$$

In Eq. (2), $X_i(t)$ denotes the current position of the individual. $\gamma \in [0, 1]$ means a random No. generated by a normal distribution. X_{best} refers to the historical global optimal position. The fitness function $f(X_i)$ is given by Eq. (3).

$$f(X_i) = P_{out}(X_i) \tag{3}$$

In Eq. (3), P_{out} is the output power of the PVA at the corresponding operating point X_i.

In intelligent optimization algorithms, the construction of the initial population has a significant impact on subsequent search efficiency and solution quality. Traditional LSO algorithms typically generate initial individuals through random means. This approach can easily lead to uneven distribution of individuals and cannot effectively cover the entire solution space, thereby limiting the algorithm's global search capability [21] [22]. Chaotic sequences have significant advantages in improving initialization quality and avoiding falling into local optima due to their good traversal and uniform distribution characteristics. Therefore, this study introduces the TCM method to optimize the position information of different types of lions in the initial population, thereby improving the overall search efficiency and global optimization ability. The calculation is shown in Eq. (4).

$$x_{n+1} = \begin{cases} 2x_n 0 \le x_n < 0.5 \\ 2(1-x_n) 0.5 \le x_n \le 1 \end{cases} \tag{4}$$

In Eq. (4), x_n is a chaotic sequence. Young lions usually adopt a fixed equal probability strategy when choosing to follow the lion king, lioness, or expelled individuals for position updates, which lacks adaptive adjustment and can easily lead to a lack of directionality when searching. To enhance the guidance and stage adaptability of search, this study introduces DPM to improve the position update strategy for young lions and proposes a new position update formula, as shown in Eq. (5).

$$x_i^{k+1}\begin{cases}\dfrac{g^k+p_i^k}{2}(1+\alpha_c\gamma) & 0<q\le u_1\\ \dfrac{p_i^k+p_m^k}{2}(1+\alpha_c\gamma) & u_1<q\le u_2\\ \dfrac{g_k'+p_i^k}{2}(1+\alpha_c\gamma) & u_2<q\le u_3\end{cases} \tag{5}$$

In Eq. (5), x_i^{k+1} is the position vector of the i-th juvenile lion in the $k+1$ th generation. p_i^k is the historical best position of the i-th individual and k -th generation in the lion pack. g^k is the optimal location for the k-generation population. p_m^k represents the historical optimal position of the $m-th$ young lion close to the lioness in the k-th generation. α_c and q are the disturbance and probability factors of the lioness. g_k' is the location where the i-th lion cub was driven away within the hunting range. u_1, u_2, and u_3 are the probabilities of the i-th cub following the lion king, lioness, and being expelled. To ensure that the algorithm strikes a balance between global exploration and local exploration, the research conducted calibration and sensitivity analysis on the value ranges of u_1, u_2, and u_3, u_1, u_2, and u_3 satisfy the constraint condition that $u_1+u_2+u_3=1$. In the parameter calibration stage, the study first sets up multiple candidate combinations and conducts 20 independent experiments on the training set and the test set, respectively, and calculates their average fitness values and the number of convergence iterations. Both the training set and the test set data are sourced from a PVP station in Sichuan Province. The data cover various working conditions, such as different time periods, different light intensities, and temperatures, and can accurately reflect the performance of the PV system under different operating conditions. Subsequently, the sensitivity analysis is conducted using the single-factor perturbation method. Under the condition of fixing two parameters, the third parameter is perturbed, with the perturbation range set to [0.2, 0.6] and the step size to 0.1, and its normalized sensitivity index is calculated. When perturbing each parameter, the training set is used to calculate the fitness value under each parameter combination, while the test set is used to verify the performance of this combination on unseen data to ensure that overfitting does not occur and that the parameter combination has good generalization ability. The formula for calculating the normalized sensitivity index S_{u_i} is shown in Eq. (6).

$$S_{u_i}=\frac{\Delta F/F}{\Delta u_i/u_i} \tag{6}$$

In Eq. (6), F represents the optimal fitness value, and Δu_i is the amplitude of parameter disturbance. $S_{u_1}\approx 0.35, S_{u_2}\approx 0.33, S_{u_3}\approx 0.12$, indicating that u_1 and u_2 have a more significant impact on the global search and convergence speed, while the influence of u_3 within a reasonable range is relatively weak. Based on this, the study ultimately adopted the parameter combination of $(u_1,u_2,u_3)=(0.4,0.4,0.2)$. Based on the above improvement strategies, this study proposes a new energy DC microgrid ESC strategy based on an improved LSO algorithm.

2.2 Hybrid ESP Allocation Strategy Based on VMD-GWO

The ESC strategy for new energy DC microgrids built on an improved LSO algorithm can effectively achieve efficient MPPT of the system. However, the fluctuation of the load side state during the operation of independent PVP generation systems can also lead to power instability [23]. To achieve collaborative regulation of energy storage components with different dynamic response speeds, this study first constructs a photovoltaic DC microgrid system based on hybrid energy storage. Secondly, by further combining VMD and GWO, a hybrid ESP allocation strategy built on VMD-GWO is established. The essence of VMD is to build and address variational issues. The expression for the calculation process of constructing variational problems is given by Eq. (7).

$$\min_{\{u_k\},\{w_k\}}\left\{\sum_k\left\|\partial_t\left[\left(\delta(t)+\frac{j}{\pi t}\right)*u_k(t)\right]e^{-jw_kt}\right\|_2^2\right\} \tag{7}$$

In Eq. (7), u_k means the set of various IMF. w_k is the set of center frequencies for each IMF. $\delta(t)$ is a Dirac function. $\left(\delta(t)+\frac{j}{\pi t}\right)$ is the result of Hilbert transform. ∂_t is the weight coefficient. k is the amount of decomposed modes. The calculation process for solving variational problems is shown in Eq. (8).

$$\begin{aligned}L\left(\{u_k\},\{w_k\},\lambda\right)=\bar{\alpha}\sum_k\left\|\partial_t\left[\left(\delta(t)+\frac{j}{\pi t}\right)*u_k(t)\right]e^{-jw_kt}\right\|_2^2\\ +\left\|f(t)-\sum_k u_k(t)\right\|_2^2+\left\langle\lambda(t),f(t)-\sum_k u_k(t)\right\rangle\end{aligned} \tag{8}$$

In Eq. (8), L is the Lagrangian function. $\bar{\alpha}$ and λ are quadratic penalty functions and Lagrange multipliers. f is the initial signal. $\langle\cdot\rangle$ is an inner product operation. The power balance constraint formula is given by Eq. (9).

$$P_{PV}+P_{BAT}+P_{SC}=P_{Load}+P_{Loss} \tag{9}$$

In Eq. (9), P_{PV} represents the PVP generation. P_{BAT} and P_{SC} are the power provided/absorbed by the battery and supercapacitor. P_{Load} is the load power. P_{Loss} is the system power loss. This study uses a Bidirectional Buck/-Boost Converter (BiBBC) as the power regulation interface

to achieve bidirectional energy flow between energy storage units. The topology structure of the BiBBC circuit is shown in Fig.3.

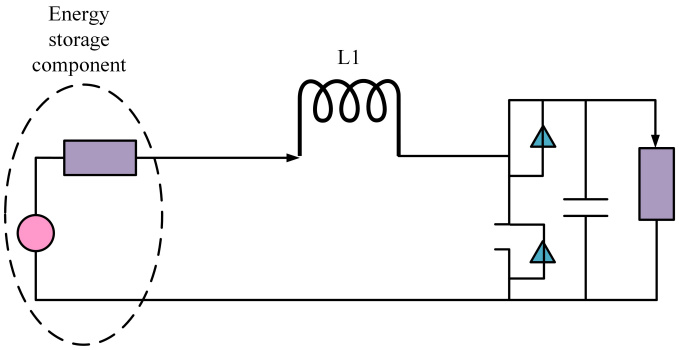

Figure 3. BiBBC Circuit Topology

In Fig.3, the BiBBC achieves opposite and complementary switching states through complementary Pulse Width Modulation (PWM) signals [24]. By programming different switch states, this converter can switch between forward boost and reverse buck modes, with energy transmitted and stored through inductors. The specific switch changes of the BiBBC are listed in Table 1.

The overall structure of a photovoltaic DC microgrid system based on a hybrid ESC is shown in Fig.4.

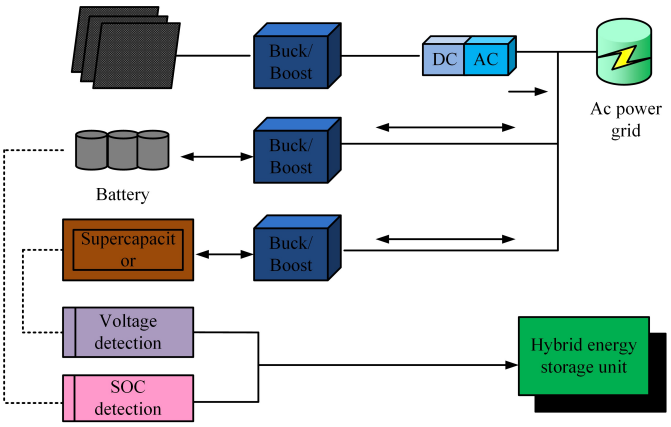

Figure 4. Structural Schematic of a Photovoltaic DC Microgrid System with Hybrid ESC Integration

In Fig.4, the PVA adopts an ESC strategy based on an improved LSO to achieve the maximum power output of PVP generation. When there is sufficient sunlight and excess electricity or low load demand, the excess electricity is transmitted to the ESD for storage via the step-down mode of the BiBBC. When the lighting is insufficient or the load demand increases, the ESD releases energy and supplements the load through boost mode to maintain system energy balance. Independent BiBBCs are installed between the ESD and the DC bus to achieve mutual isolation and precise control, ensuring the coordinated operation of the battery and supercapacitor. Through reasonable energy management strategies, the system can effectively smooth out voltage and power fluctuations and improve operational safety. When the external environment or load changes cause power fluctuations, the power allocation module adjusts the C&D of each ESD according to the strategy, achieving stable DC bus power and meeting load requirements.

The selection of the number K for VMD decomposition will directly affect the decomposition effect. If the value is too small, it can easily lead to mode mixing and ineffective extraction of HF components. If the value is too large, redundant components may appear. To avoid the irrationality caused by human settings, this study uses GWO to optimize the IMF decomposition amount and VMD's penalty factor, to improve the power allocation efficiency of the hybrid ESC system. The optimization process is shown in Fig.5.

In Fig.5, a fitness function that can effectively measure the quality of power signal decomposition is first constructed as an evaluation criterion in the optimization process. Subsequently, GWO is employed to randomly initialize the population individuals, ensuring the breadth and diversity of the search space coverage. Under the initial population parameter setting, the power signal of the hybrid ESC system is subjected to VMD, and the fitness related to each individual is calculated based on the decomposition results. Subsequently, based on fitness ranking, the three gray wolves with the best fitness are chosen as the leader individuals and their positions in the search space are recorded. Next, the algorithm simulates the social hierarchy structure in the gray wolf population, sequentially performing behaviors such as tracking prey, surrounding prey, and launching attacks, to update the population position and generate a new generation of individuals. If the termination condition is met, the optimal parameter combination will be output; otherwise, it continues iterating until convergence. The distance D between prey (global optimal solution) $X_p(t)$ and grey wolf X (potential solution space) is shown in Eq. (10).

$$D = |C * X_p(t) - X(t)| \tag{10}$$

In Eq. (10), C is the coefficient vector. The correlation degree r_i between vectors is shown in Eq. (11).

$$r_i = \frac{1}{n}\sum_{k=1}^{n}\xi_i(k) \tag{11}$$

In Eq. (11), $\xi_i(k)$ is the correlation coefficient between each parameter and the corresponding parameter of the reference sequence. n is the length of the time series. In the process of VMD parameter optimization, the fitness function adopts the weighted sum form of energy entropy and normalized reconstruction error to evaluate the decomposition quality. Among them, energy entropy is used to measure the degree of energy distribution of each modal component. The smaller the value, the stronger the independence between modes and the clearer the decomposition effect. The reconstruction error is used to measure the difference between the decomposed signal and the original signal. The smaller the value, the more complete the signal features are retained. By comprehensively considering both energy concentration and reconstruction accuracy, it

Table 1
BiBBC Switching Variation

Serial number	Switching mode S_1	Refill diode D_1	Switching mode S_2	Refill diode D_2
1	Conduction	Deadline	Turn off	Deadline
2	Turn off	Deadline	Conduction	Continuous flow
3	Turn off	Deadline	Conduction	Deadline
4	Conduction	Continuous flow	Turn off	Deadline

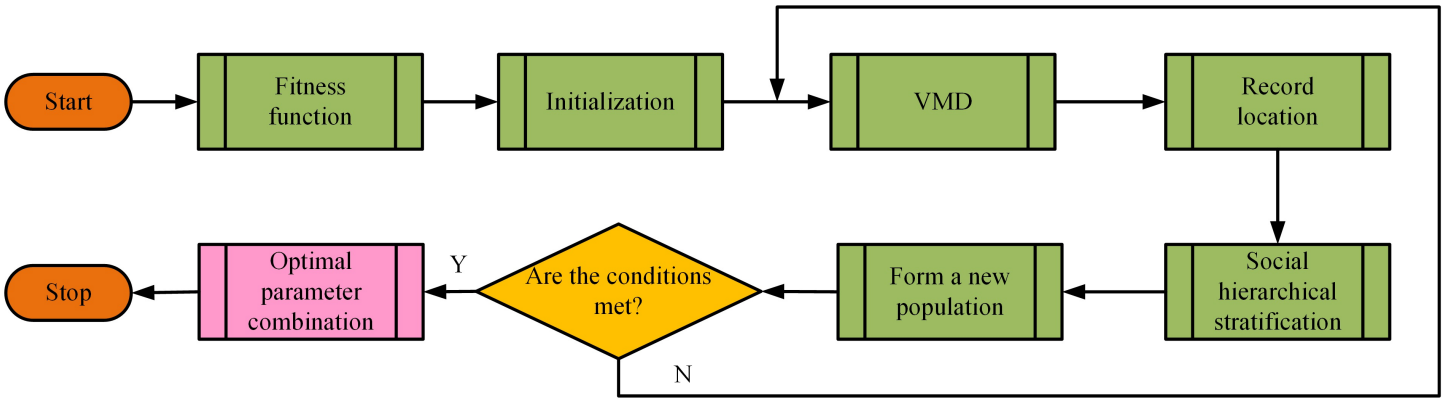

Figure 5. VMD-GWO Algorithm Flow Diagram

is possible to ensure the stability of decomposition while avoiding information loss, thereby obtaining the optimal decomposition parameter configuration. The calculation formula of the fitness function L' is shown in Eq. (12).

$$L' = w_1 \cdot H + w_2 \cdot N + w_3 \cdot C_{pen} \tag{12}$$

In Eq. (12), H represents the normalized energy entropy, N is the normalized reconstruction error, and C_{pen} is the complexity penalty term, which is used to prevent the decomposition result from being overly complex. The weight coefficients w_1, w_2 and w_3 satisfy $w_1 + w_2 + w_3 = 1$. In the experiment, the weight coefficients $w_1 = 0.55, w_2 = 0.40$, and $w_3 = 0.05$ are selected. This weight selection is based on theoretical analysis and verified through sensitivity analysis and optimization experiments. The w_1 value (0.55) prioritizes energy entropy, aiming to ensure higher independence among various modes, avoid overlap and aliasing, and enhance the clarity of decomposition. The w_2 value (0.40) pays more attention to the reconstruction error to ensure that the decomposed signal can retain the key features of the original signal as much as possible. The weight of w_3 is relatively small (0.05), mainly used to limit the complexity of the decomposition results and avoid generating too many unnecessary modes. Through sensitivity analysis, the experimental results show that this weight configuration can effectively balance energy concentration, reconstruction accuracy, and complexity, thereby optimizing the overall performance of the VMD algorithm.

To further clarify and improve the synergistic effect of LSO and VMD-GWO in the control of DC microgrids, the study aims to closely integrate the two into the control cycle in the method design to achieve efficient linkage between MPPT and power decomposition/energy storage allocation. The specific process is shown in Fig.6.

As shown in Fig.6, first of all, the instantaneous DC

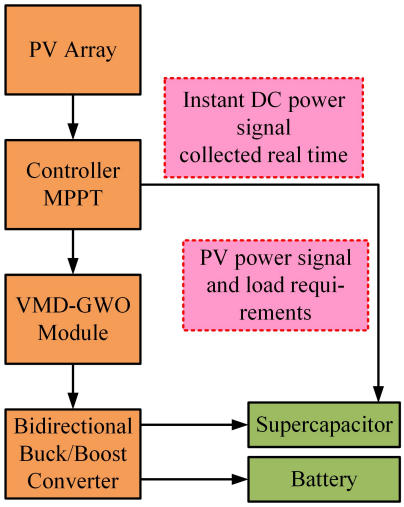

Figure 6. MPPT and Power Decomposition/Energy Storage Allocation Process

power signal output by the PVA is collected in real time by the controller. The improved LSO quickly calculates and outputs the MPPT based on the current environmental conditions and historical optimal solutions to ensure that the photovoltaic system can achieve global optimal power generation under any lighting conditions. Subsequently, the obtained PVP signals and load demands are sent to the VMD-GWO module for frequency-domain decomposition and parameter optimization. The VMD decomposes the power signals into high-frequency and low-frequency modes. The GWO optimizes the decomposition parameters to ensure the minimization of energy entropy and the minimum reconstruction error, thereby obtaining power distribution strategies suitable for different energy storage units. Ultimately, the BiBBC controls the C&D of

the supercapacitor and the battery, respectively, based on the high- and low-frequency power signals output by VMD-GWO, achieving the smoothing of power fluctuations and the extension of the life of the energy storage system.

3. Results

3.1 Simulation Testing of ESC Strategy for New Energy DC Microgrid

The simulation modeling of each module of the standalone PVP generation system is completed in the Matlab/Simulink software. The ambient temperature is set at $25°C$, the standard light is 950 W/m^2, the power of the PVA is 5 kW, the capacity of the battery is 200 kWh, the capacity of the supercapacitor is 50 kWh, and the system load varies randomly from 3 kW to 6 kW. To further enhance the practical application reliability of the proposed ESC strategy, the study also introduces a Hardware-in-the-Loop (HIL) test verification scheme outside the simulation environment. In the HIL test, the BiBBC is controlled by real power switching devices (IGBT/MOSFET), and the energy storage unit model is implemented in real-time through FPGA for control logic calculation and PWM signal generation to ensure that the controller response is consistent with the actual hardware. The PVP signal is transmitted from Matlab/Simulink to the FPGA through a high-speed data interface. After control and calculation, it drives the switch state of the converter to achieve real-time C&D of the energy storage unit. This HIL configuration can truly reflect the dynamic response and circuit delay of switching devices, thereby more accurately evaluating the dynamic performance, steady-state error, and power allocation efficiency in the actual power grid environment. Under standard lighting conditions, the changes in output power of PSO, conductance increment method, LSO, and research algorithms are shown in Fig.7.

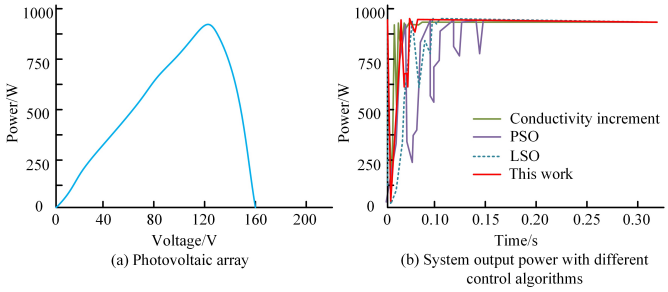

Figure 7. Variation of System Output Power Under Standard Light Conditions

Fig.7 (a) displays the OPC of the PVA in standard lighting conditions. Fig.7 (b) is the variation of system output power under different control algorithms. Under standard lighting conditions of 950 W/m^2, the photovoltaic system only has one MaxPP, which is 860 W. At this point, the tracking process of the MaxPP is relatively stable. The maximum power tracking value of LSO is 857.3 W, with a time consumption of about 0.06 s and an accuracy of 99.69%. However, there are significant power fluctuations in the initial stage, indicating weak robustness to disturbance signals. The research algorithm introduces a better parameter adaptive adjustment mechanism in the processing, significantly speeding up the search process. It can complete tracking within 0.04 seconds, reaching a maximum power value of 859.2 W and improving tracking accuracy to 99.91%. In addition, compared with the PSO and conductance increment method, the research algorithm has a smaller fluctuation amplitude and faster response in the dynamic tracking process, effectively reducing the impact of system power jitter on DC bus stability. This further enhances the overall reliability of the system under islanding operation mode. Under the condition of partial obstruction in the external environment, that is, when two PVAs are respectively affected by uneven irradiation intensities of about 750 W/m^2 and 550 W/m^2, the changes in power output of different control algorithms are shown in Fig.8.

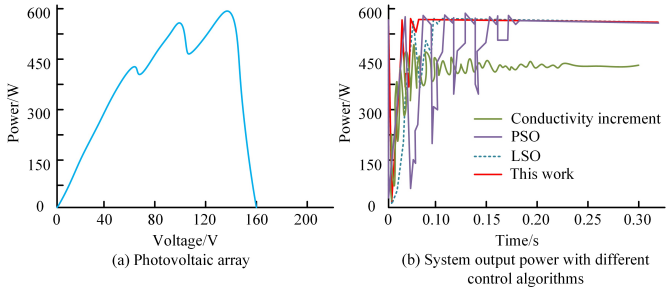

Figure 8. Variation of System Output Power Under Partial Shading Conditions

Fig.8 shows the OPC of the PVA under partial occlusion conditions and the changes in system output power under different control algorithms. When there is occlusion, the system power output curve exhibits multiple local peaks and a unique global MaxPP, with a global maximum power of 582.1 W. Compared with standard lighting, this complex lighting distribution significantly increases the complexity of MPPT and the risk of falling into local optima. The maximum power of the LSO is 578.2 W, taking about 0.09 s, and the tracking accuracy is 99.33%. However, there are still multiple severe oscillations during the initial optimization stage, resulting in a decrease in the energy utilization efficiency of the system. The research algorithm completes the MaxPP positioning within 0.064 s, with a power value of 581.6 W and a tracking accuracy of 99.91%. Its shorter response time and higher steady-state accuracy are attributed to the optimized search mechanism, which better avoids local extremum interference. At the same time, the algorithm's global optimization ability and dynamic response stability under non-ideal operating conditions have been improved, effectively enhancing the system's energy output efficiency and anti-interference performance. Assuming that the system is in a partially occluded state at the initial moment, one of the PVAs receives an irradiation intensity of 820 W/m^2. When running for 0.3 seconds, the light intensity suddenly decreases to 620 W/m^2 due

to environmental interference. At this time, the dynamic change curve of output power is shown in Fig.9.

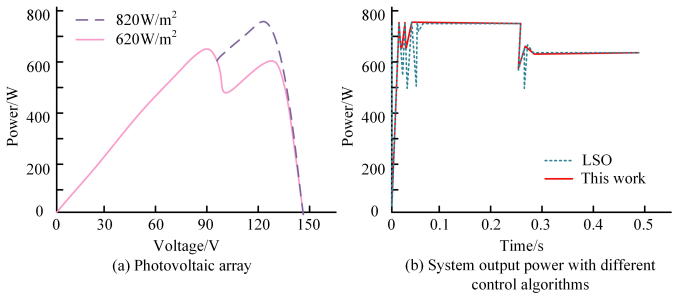

Figure 9. Variation of System Output Power Under Dynamic Illumination

Fig.9 (a) is the OPC of the PVA in dynamic conditions, and Fig.9 (b) exhibits the variation of system output power under different control algorithms. Within 0 s-0.3 s, the system power output reaches the global maximum of 728.5 W, but when the lighting suddenly changes, the new MaxPP drops sharply to 615.6 W. When using traditional LSO, the system completes the positioning of the new power point in about 0.38 s, with a maximum output power of 612.2 W, a tracking time of about 0.08 s, and an accuracy of 99.45%. However, there are frequent oscillations and significant energy fluctuations during the process. The research algorithm can achieve tracking of the new MaxPP within 0.35 s, reaching a power peak of 614.9 W and improving tracking accuracy to 99.89%. Compared with others, the research algorithm has shown significant advantages in response speed, dynamic stability, and oscillation control. The research algorithm can also demonstrate superior dynamic performance and robustness in complex operating scenarios with rapid changes in light intensity, effectively ensuring the continuity and reliability of energy output of photovoltaic systems under islanded operating conditions.

3.2 Simulation Testing of Hybrid ESP Allocation Strategy

This study selects the measured photovoltaic output power data of a PVP station in Sichuan Province from 5:00 am to 9:00 pm on a certain day as the analysis object. The sampling interval is set to once every 5 s, and a total of 11,898 records are obtained, which are divided into training and testing sets in an 8:2 ratio. This study first explores the optimal parameter combination for the hybrid ESP allocation strategy based on VMD-GWO, as shown in Fig.10.

Figs.10 (a) and (b) show the changes in fitness values of the VMD-GWO algorithm in the training and testing sets. When the number of modes is less than 6, high- and low-frequency signals are prone to aliasing. When the number of modes is greater than 6, redundant modes will be generated, reducing the decomposition efficiency. Therefore, choosing a modal number of 6 can achieve a reasonable energy distribution and ensure the stability of decomposition. For the penalty factor, if its value is too small, it will cause

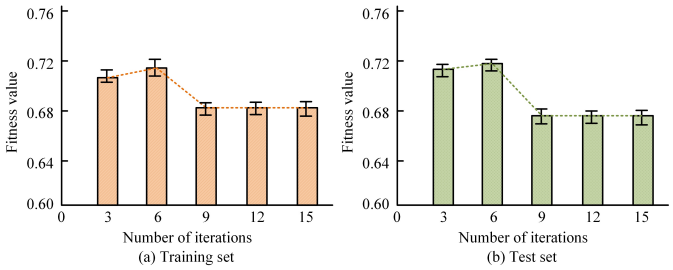

Figure 10. VMD-GWO Algorithm Fitness Curve

spectral overlap; if it is too large, it will make the signal overly smooth. Through fitness optimization calculation, it is found that when the penalty factor is 2,350, the minimum fitness values are obtained on both the training set and the test set, which can ensure the accuracy and stability of the decomposition. This parameter combination can effectively extract the high- and low-frequency features of PVP data and improve the reliability of prediction. Ultimately, the VMD-GWO algorithm reaches the minimum fitness function value in the 9th iteration, and the optimal parameter combination is determined as the number of modes being 6 and the penalty factor being 2,350. Based on the optimal parameter combination, this study decomposes the power curve of the hybrid ESC system through VMD, and the center frequencies of each IMF obtained after decomposition are exhibited in Table 2.

Table 2
IMF Centre Frequency

IMF component	Centre frequency $\times 10^{-3}/Hz$	Energy storage unit
IMF-1	0.16	Supercapacitor
IMF-2	0.39	Supercapacitor
IMF-3	0.55	Supercapacitor
IMF-4	0.90	Battery
IMF-5	1.21	Battery
IMF-6	1.53	Battery
IMF-7	1.85	Battery
IMF-8	2.26	Battery
IMF-9	3.02	Battery

In Table 2, the study decomposes the power signal of the PV system in the frequency domain through VMD and optimizes the VMD parameters by using GWO. Eventually, the IMFs of different frequency bands from IMF1 to IMF9 are obtained, with each IMF representing a different frequency band in the signal. The central frequency distribution among each modal component is clear, and the frequency band distinction is distinct, demonstrating excellent decoupling capability. Meanwhile, the degree of aliasing between components is effectively evaluated by minimizing energy entropy as the criterion. During the application process, the IMFs in the ultra-high frequency section (such as IMF1-IMF3) are mainly allocated to supercapacitors to cope with rapidly changing power fluctuations. The low-frequency IMFs (such as IMF4-IMF8) are mainly allocated to the battery to handle relatively stable

Table 3
Multi-Source Fluctuation Scenario Test Results

Methods	Bus voltage fluctuation rate/%	Current THD /%	Energy allocation error/%	Power balance recovery time/s	Storage utilization rate /%
LPF	3.8	5.6	6.2	0.92	84.7
PID	3.2	4.9	5.1	0.78	87.3
PSO	2.5	3.7	3.8	0.63	90.4
This work	2.1	3.1	2.6	0.47	93.1

power demands. The specific frequency allocation basis is as follows: For all IMF components, those exceeding a certain center frequency can be regarded as the high-frequency part and allocated to the supercapacitor energy storage unit. The IMF component lower than the central frequency is regarded as the low-frequency part and is allocated to the battery energy storage unit. This distribution strategy enables supercapacitors to respond quickly to high-frequency fluctuations, while batteries can effectively and stably output long-term power demands. To further verify the applicability of VMD-GWO in hybrid ESC systems, the paper also selects an LPF algorithm as a control and processes the same hybrid power signal separately. Subsequently, the processed results are used for power allocation between two different energy storage units, as shown in Fig.11 for comparison.

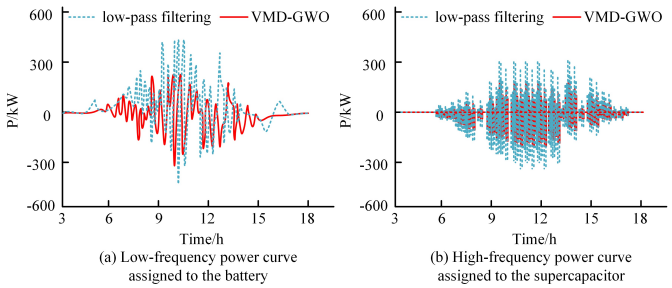

Figure 11. LF Power vs. HF Power Curves

Figs.11 (a) and (b) show the LF and HF power curves allocated to the battery and supercapacitor. When using traditional LPF methods within the same operating time, the maximum power for the C&D the battery pack is 348.6 kW and 375.1 kW. After adopting VMD-GWO, the maximum charging power of the battery pack is 318.7 kW, and the maximum discharging power drops to 241.5 kW. This indicates that VMD-GWO has higher resolution in high- and low-frequency power separation, significantly reducing the frequency of power fluctuations allocated to the battery and minimizing energy loss caused by frequent C&D of the battery pack. The reduction of C&D depth not only alleviates power shock but also plays a positive role in extending the service life of the battery. In addition, VMD-GWO can allocate higher frequency and larger instantaneous power changes to supercapacitors with fast response speed and long cycle life, allowing both types of ESDs to operate within their optimal operating range. To test the adaptability and stability of the proposed control method under complex fluctuation conditions, the wind speed variation range is set at 6 m/s to 12 m/s in the study, and the wind speed sudden change and random disturbance signals are superimposed to simulate the rapid fluctuation of wind power output. The photovoltaic section still operates under three types of conditions: standard lighting, local shading, and dynamic lighting. By superimposing the input of photovoltaic and wind power, a typical multi-source coupled fluctuation scenario is designed. Among them, the base value of wind power varies over time according to the average power curve, while a random disturbance signal is superimposed. This disturbance follows the Gaussian white noise with a mean of 0 and a standard deviation of 5% of the rated power. In addition, to simulate sudden power changes, a power jump event is set up, with a change rate of 0.8 kW/s. The duration of each jump is random, conforming to the Poisson distribution (with an average interval of 30 s). The wind power curve generated by this method has both gradual change and randomness, which can effectively reflect the uncertainty and rapid fluctuation characteristics of wind power output in the actual microgrid, thereby ensuring that the simulation results of the power distribution strategy can be repeatedly verified. The test results are shown in Table 3.

In Table 3, in the multi-source coupled fluctuation scenario, the research method performs outstandingly in multiple indicators. Firstly, the voltage fluctuation of the DC bus is controlled at 2.1%, which is approximately 45% lower than that of the traditional LPF, effectively enhancing the voltage stability of the system. Secondly,the Total Harmonic Distortion rate (THD) of the current has decreased from 5.6% to 3.1%, indicating that this method has a better power quality guarantee capability in a rapidly fluctuating environment. The energy distribution error is reduced to 2.6%, significantly superior to the PID and PSO methods, indicating that the VMD-GWO algorithm is more accurate in decoupling high- and low-frequency energy and division of labor in energy storage units. The power balance recovery time has been shortened to 0.47 s, and the response speed has nearly doubled, enabling faster response to sudden changes in photovoltaic and wind power output. Finally, the energy storage utilization rate increases to 93.1%, indicating that the research method not only improves the rationality of energy distribution but also enhances the overall operational efficiency of energy storage equipment. In the complex fluctuation scenario of multi-source coupling, the research method still has strong stability, robustness, and energy management capabilities, and can effectively coordinate the dynamic fluctuations of photovoltaic and wind power output, providing a strong guarantee for the safe, reliable, and efficient operation of

microgrids.

To further evaluate the impact of the hybrid ESP distribution strategy on battery life under long-term operation, a preliminary battery attenuation model is introduced in the experiment to simulate the influence of continuous charge-discharge cycles on capacity attenuation. In the experiment, the HIL system is subjected to continuous cycle C&D under standard illumination (950 W/m^2), partial occlusion (550 W/m^2-750 W/m^2), and dynamic illumination variation (500 W/m^2-820 W/m^2) conditions. Each cycle lasts for 30 minutes, with a total of 50 cycles. The battery voltage, the C&D power, and the amplitude of power fluctuation are recorded. The test results are shown in Table 4.

In Table 4, with the increase of the number of Charge and Discharge Cycles (CDCs), the maximum C&D power of the battery and the amplitude of power fluctuation show a slight downward trend. The initial capacity attenuation is approximately 2% after 50 cycles, indicating that the proposed hybrid ESP distribution strategy has a limited impact on battery performance in the short term. Based on the HIL experimental results, the efficiency of the control algorithm in power distribution and its inhibitory effect on the C&D shock of the battery can be verified. At the same time, it provides an experimental basis and data support for the subsequent complete battery life attenuation modeling and long-term operation feasibility analysis. Finally, the system performance test of the proposed VMD-GWO hybrid ESP distribution strategy is conducted in the photovoltaic DC microgrid environment. The rated power of the PVA is set at 5 kWp, with a peak output of approximately 4.8 W. The load simulates household electricity usage, with a peak power of about 3 kW. The energy storage adopts a 48 V, 100 Ah lithium-ion battery pack, with a sampling frequency of 1 Hz. The MPPT and ESP distribution strategy are executed in real-time through the controller. Traditional LPF, PID-based control strategy, and PSO are introduced as comparison methods. The experimental period is 16 h/d (05:00-21:00) for 7 consecutive days, and the average value is taken for analysis. The recorded indicators include the number of CDCs, the range of SOC variation, the Maximum Power Tracking Error (MPTE), the Fluctuation of Battery Terminal Voltage (FBTV), the Efficiency of the Energy Storage System (EESS), the Peak Load Response Time (PLRT), and the Total Energy Utilization Rate (TEUR) of the system. The experimental results are shown in Table 5.

Table 5 shows that the hybrid ESP distribution strategy based on VMD-GWO outperforms other methods in multiple indicators. Compared with the traditional LPF and PID control methods, the reduction in the number of CDCs is 54% and 45%, respectively. The SOC fluctuation range is more reasonable, the battery terminal voltage fluctuation is the smallest, and the MPTE is the lowest. The EESS and the TEUR of the system have been significantly improved, and the PLRT has been shortened. This indicates that this strategy can smooth the power output of energy storage, enhance the system response speed and operational stability, and reduce the frequency of battery C&D, thereby effectively extending the battery life and optimizing the overall energy utilization level of the microgrid.

4. Conclusion

This study proposed a hybrid ESC method based on improved LSO and VMD-GWO algorithms to address slow energy storage response, uneven power distribution, and severe voltage fluctuations in new energy DC microgrids. This method improved the MPPT accuracy of the LSO by optimizing its global search performance. Meanwhile, by utilizing GWO to optimize the VMD, the mixed power signal was decomposed into high and low frequency components, achieving precise power matching and coordinated scheduling of supercapacitors and batteries. A large amount of simulation data showed that under different sunshine conditions and load disturbances, the stability of the system bus voltage and energy scheduling efficiency were significantly better than traditional methods. Under dynamic conditions, the research method could achieve tracking of the new MaxPP within 0.35 s, reaching a power peak of 614.9 W and improving tracking accuracy to 99.89%. In addition, within the same operating time, the maximum charging power of the battery pack was 318.7 kW, and the maximum discharging power decreased to 241.5 kW.

To evaluate the real-time feasibility of the proposed improved LSO algorithm and VMD-GWO algorithm in the actual microgrid control, a quantitative analysis of the computing time of both was conducted in the study. The improved LSO algorithm was used for MPPT. Under standard lighting conditions, the average computing time for completing one iteration was approximately 0.0015 s. Within 20 to 30 iterations, the entire MPPT process could be completed within 0.04 s to 0.05 s, which was much shorter than the sampling period of the DC microgrid (0.1 s), meeting the real-time control requirements of the system. The VMD-GWO algorithm was used for the optimization of power allocation in hybrid energy storage. The average time consumption for a single VMD decomposition and GWO iteration (population size 30, maximum number of iterations 10) was approximately 0.28 s, which was still within an acceptable range compared with the system sampling period. When the power distribution update frequency was set to 1 s or longer, the impact of its computing delay on the dynamic performance of the system was relatively small. Further analysis showed that the improved LSO algorithm, due to the adoption of TCM and dynamic probability factor optimization, increased the iterative convergence speed by approximately 20%, significantly reducing the computational overhead. The VMD-GWO algorithm reduced redundant modal calculations by optimizing the number of IMFs and penalty factors, making the GWO search iteration more efficient. Based on the HIL test results, the research method could complete the power tracking and distribution calculation under dynamic light changes within 0.35 s, which not only ensured the real-time performance of DC microgrid ESC but also

Table 4
HIL Cycle Experiment and Preliminary Capacity Attenuation Analysis

Number of cycles	Maximum charging power of the battery /kW	Maximum discharge power of the battery /kW	Power fluctuation amplitude /kW	Predict capacity attenuation /%
0	318.7	241.5	12.3	0.0
10	316.2	239.8	12.5	0.4
20	313.9	237.9	12.7	0.8
30	311.7	235.6	12.9	1.2
40	309.5	233.4	13.1	1.6
50	307.2	231.0	13.4	2.0

Table 5
Multi-index Performance Testing

Methods	CDC/day	SOC fluctuation range /%	MPTE/%	FBTV/V	EESS/%	PLRT/s	TEUR/%
LPF	48	20-80	5.2	1.8	88.5	0.85	81.3
PID	40	25-78	4.1	1.5	90.1	0.72	83.9
PSO	28	28-76	2.8	1.1	91.5	0.55	87.2
This work	22	30-75	2.1	0.9	93.2	0.42	90.5

maintained high-precision MPPT and power distribution performance.

In conclusion, although the meta-heuristic optimization algorithm has a large computational load, through parameter optimization and reasonable configuration of control cycles, its real-time performance in actual microgrid control can be ensured. However, this study did not fully consider physical degradation factors such as battery aging and temperature rise. Future work can further combine physical modeling with data-driven algorithms to improve the dynamic adaptive scheduling mechanism and attempt to deploy the model to embedded platforms to promote the engineering application of real-time control and edge intelligence.

Funding

The research is supported by Liaoning Provincial Department of Education University Basic Research Projects (LJ242411632066).

References

[1] Z. H. A. Al-Tameemi, T. T. Lie, and G. Foo, "Optimal coordinated control of dc microgrid based on hybrid pso-gwo algorithm," *Electricity*, vol. 3, no. 3, pp. 346–364, 2022.

[2] J. A. Glenn and S. Alavandar, "Hybrid optimized pi controller design for grid tied pv based electric vehicle," *Intelligent Automation and Soft Computing*, vol. 36, no. 2, pp. 1523–1545, 2023.

[3] A. Asaad, A. Ali, and K. Mahmoud, "Multi-objective optimal planning of ev charging stations and renewable energy resources for smart microgrids," *Energy Science & Engineering*, vol. 11, no. 3, pp. 1202–1218, 2023.

[4] X. Mei, C. Li, and Q. Sheng, "Development of a hybrid artificial intelligence model to predict the uniaxial compressive strength of a new aseismic layer made of rubber-sand concrete," *Mechanics of Advanced Materials and Structures*, vol. 30, no. 11, pp. 2185–2202, 2023.

[5] I. Hussain, B. Singh, S. Bhattacharyya, and P. Kant, "Selective harmonic elimination–based control of ternary cascaded nine-level converter-based photovoltaic power generating system," *International Journal of Power and Energy Systems*, vol. 41, no. 2, pp. 1–9, 2021.

[6] G. D. Wu, D. G. Hu, L. J. Liu, and G. Bao, "Improved pso algorithm application research for new energy consumption in microgrid combination optimisation model," *International Journal of Power and Energy Systems*, vol. 44, no. 10, pp. 1–11, 2024.

[7] Y. Zhang, P. Wang, and H. Yang, "Optimal dispatching of microgrid based on improved moth-flame optimization algorithm based on sine mapping and gaussian mutation," *Systems Science & Control Engineering*, vol. 10, no. 1, pp. 115–125, 2022.

[8] Z. Xie and Z. Wu, "A flexible power point tracking algorithm based on adaptive lion swarm optimization for photovoltaic system," *Soft Computing*, vol. 27, no. 8, pp. 4953–4973, 2023.

[9] S. Silambarasan and M. S. Devi, "Hybrid simulated annealing with lion swarm optimization algorithm with modified elliptic curve cryptography for secured data transmission over wireless sensor networks," *International Journal of Computer Networks and Applications*, vol. 9, no. 3, pp. 316–327, 2022.

[10] K. Dinesh and S. K. Svn, "Gwo-smslo: Grey wolf optimization based clustering with secured modified sea lion optimization routing algorithm in wireless sensor networks," *Peer-to-Peer Networking and Applications*, vol. 17, no. 2, pp. 585–611, 2024.

[11] H. Liu, P. Zhang, and H. Xing, "Research on primary frequency regulation control strategy of flywheel energy storage assisted thermal power unit based on vmd decomposition," in *IET Conference Proceedings CP843*, (Stevenage, UK), pp. 784–790, The Institution of Engineering and Technology, 2023.

[12] D. Li, H. Chen, and Y. Yao, "Mdt-mvmd-based frequency modulation for photovoltaic energy storage systems," *Journal of Power Electronics*, vol. 25, no. 2, pp. 324–335, 2025.

[13] Y. Zhang, Y. Zhang, and T. Wu, "Integrated strategy for real-time wind power fluctuation mitigation and energy storage system control," *Global Energy Interconnection*, vol. 7, no. 1, pp. 71–81, 2024.

[14] G. Li, G. Tang, and X. Liu, "An internal voltage robust control of battery energy storage system for suppressing wideband harmonics in vf control-based islanded microgrids," *IEEE Transactions on Industrial Informatics*, vol. 20, no. 2, pp. 2320–2330, 2023.

[15] K. S. S. Liyakat and K. K. S. Liyakat, "Pv power control for dc microgrid energy storage utilisation," *Journal of Digital Integrated Circuits in Electrical Devices*, vol. 8, no. 3, pp. 1–8, 2023.

[16] J. Su, K. Li, and Y. Li, "A novel state-of-charge-based droop control for battery energy storage systems to support coordinated operation of dc microgrids," *IEEE Journal of Emerging and Selected Topics in Power Electronics*, vol. 11, no. 1, pp. 312–324, 2022.

[17] M. Zhang, Q. Xu, and C. Zhang, "Decentralized coordination and stabilization of hybrid energy storage systems in dc microgrids," *IEEE Transactions on Smart Grid*, vol. 13, no. 3, pp. 1751–1761, 2022.

[18] S. Punna, R. Mailugundla, and S. R. Salkuti, "Design, analysis and implementation of bidirectional dc-dc converters for hess in dc microgrid applications," *Smart Cities*, vol. 5, no. 2, pp. 433–454, 2022.

[19] X. Liu, T. Zhao, and H. Deng, "Microgrid energy management with energy storage systems: A review," *CSEE Journal of Power and Energy Systems*, vol. 9, no. 2, pp. 483–504, 2022.

[20] Y. Mi, J. Deng, and X. Wang, "Multiagent distributed secondary control for energy storage systems with lossy communication networks in dc microgrid," *IEEE Transactions on Smart Grid*, vol. 14, no. 3, pp. 1736–1749, 2022.

[21] K. S. S. Liyakat and K. K. S. Liyakat, "Pv power control for dc microgrid energy storage utilisation," *Journal of Digital Integrated Circuits in Electrical Devices*, vol. 8, no. 3, pp. 1–8, 2023.

[22] F. Badfar, A. A. Safavi, and M. M. Arefi, "Simultaneous output feedback robust model predictive control and state estimation for dc microgrids," *International Journal of Electrical Power & Energy Systems*, vol. 159, p. 110012, 2024.

[23] M. Zolfaghari, G. B. Gharehpetian, and M. Shafie-khah, "Comprehensive review on the strategies for controlling the interconnection of ac and dc microgrids," *International Journal of Electrical Power & Energy Systems*, vol. 136, p. 107742, 2022.

[24] M. Ren, X. Sun, and Y. Sun, "A virtual inertial control strategy for bidirectional interface converters in hybrid microgrid," *International Journal of Electrical Power & Energy Systems*, vol. 153, p. 109388, 2023.

Biographies

Fanhua Meng received their Bachelor's degree in Electrical Engineering from Shenyang Institute of Engineering. Since then, they have been a Master's candidate with the School of Electrical Engineering, Shenyang Institute of Engineering. Their research interests include power system analysis.

Likui Yi received their Ph.D. degree in Control Theory and Control Engineering from Northeastern University, China, in 2012. Since 2012, they have been an Associate Professor with the School of Electrical Engineering, Shenyang Institute of Engineering. Their research interests include fault monitoring of electrical equipment in power systems, new energy power generation, and grid-connected technology.

Rui Feng received their Bachelor's degree in Electrical Engineering from Shenyang Institute of Engineering. Since then, they have been a Master's candidate with the School of Electrical Engineering, Shenyang Institute of Engineering. Their research interests include the application of hybrid energy storage in primary frequency regulation.

Dongge Liu received their Bachelor's degree in Electrical Engineering from Shenyang University of Technology. Since then, they have been a Master's student with the School of Electrical Engineering, Shenyang University of Technology. Their research interests include power system analysis and modern control theory.